INTERNATIONAL JOURNAL OF HYDROGEN ENERGY 39 (2014) 13285–13291

Available online at www.sciencedirect.com

ScienceDirect

journal homepage: www.elsevier.com/locate/he

Differential diffusion effects in numerical simulations of laminar, axi-symmetric H_2/N_2–air diffusion flames

G. Maragkos [a,*], P. Rauwoens [b], B. Merci [a]

[a] Department of Flow, Heat and Combustion Mechanics, Ghent University, St. Pietersnieuwstraat 41, B-9000 Ghent, Belgium

[b] Department of Civil Engineering, Ghent University, Technology Park 904, B-9052 Ghent, Belgium

ARTICLE INFO

Article history:
Received 8 May 2014
Received in revised form
11 June 2014
Accepted 15 June 2014
Available online 17 July 2014

Keywords:
Laminar flame
Differential diffusion
Hydrogen

ABSTRACT

The accuracy of a new methodology to include differential diffusion in numerical simulations of reactive flows is illustrated for a set of laminar, axi-symmetric H_2/N_2–air diffusion flames. From the comparison of the calculations with the experimental data it is observed that when differential diffusion effects are properly taken into account in the transport equations in physical space, simulation results agree well with the experimental data. Ignoring differential diffusion effects is not acceptable, due to lack of H_2 diffusion close to the jet inlet. Overall, differential diffusion has a strong influence on the stabilization of the flame as well as on the chemical species concentrations.

Introduction

Numerical simulations of reactive flows typically involve mixtures of different chemical species, each one with different properties. Hydrogen is a much lighter chemical specie when compared to other chemical components (e.g. CO_2, N_2 or O_2). This much smaller molecular weight of hydrogen causes it to behave differently from the other chemical species in a mixture. More in particular, it diffuses faster than other chemical species, e.g. CO_2. Indeed, the species molecular diffusion controls mixing, thus chemical reactions. If differential diffusion effects are taken into account, the local species concentrations, heat release rates and flame temperatures strongly differ from the ones predicted by the equal diffusivity assumption [1], especially when mixtures of species with vastly different diffusivities (such as H_2) are to be considered. Yet, differential diffusion effects are often ignored when performing numerical simulations of reactive flows because it leads to great modeling simplifications. In addition to assuming equal mass diffusivities for all chemical species, another common assumption is to consider equal thermal and mass diffusivities, leading to unity Lewis number for all chemical species. These two assumptions then lead to the definition of a conserved scalar, the mixture fraction, which uniquely describes the transport of species [2]. By making use of conserved scalars (scalars whose value does not vary during

* Corresponding author.
E-mail address: Georgios.Maragkos@UGent.be (G. Maragkos).
http://dx.doi.org/10.1016/j.ijhydene.2014.06.086

a chemical reaction) the solution of the flow is decoupled from the chemical reactions. However, as stated, the mathematical derivation relies upon the assumption that all chemical components diffuse equally, which in reality is not the case.

The influence of differential diffusion on the structure of laminar hydrogen–air diffusion flames has been the focus of several numerical studies in the past. The differential diffusion effects on species and heat in a $H_2/CH_4/N_2$–air flame were examined in Ref. [3], while temperature fields of regular and inverse diffusion flames, taking into account detailed chemical kinetics and multi-component diffusion, were presented in Ref. [4]. The effects of non-unity Lewis number and finite rate chemistry on the dynamics of a H_2–air diffusion flame were reported in Ref. [5] while the influence of chemical non-equilibrium effects in hydrogen–air jet diffusion flames, using detailed chemistry and multi-component diffusion, were presented in Ref. [6]. There also exist combined numerical and experimental studies examining the structure of laminar hydrogen–air diffusion flames with the inclusion of thermal diffusion [7–9].

The goal of this numerical study is to apply the recently presented methodology [10] to include differential diffusion effects in CFD simulations of reactive flows, to a set of laminar, axi-symmetric H_2/N_2–air diffusion flames, illustrating the accuracy of the method to reproduce the influence of differential diffusion in laminar flames. To that purpose, comparisons are made with experimental data, including (or not) differential diffusion of species and heat in the simulations.

Experimental set-up

The experiments reported by Toro et al. [7] are considered. The mixture of H_2/N_2 (1:1 in mole ratio), issued into air by a round tube of inner diameter $d = 0.9$ cm, is surrounded by a co-flow of air (inner diameter 9.5 cm). The inflow of the mixture, located in the center of the bottom plane, is positioned 0.8 cm above the exit of the co-flow. Three average velocities with parabolic profile are considered: 18, 27 and 50 cm/s. The inlet velocity of the co-flow is set at the average exit velocity of the mixture. Ambient temperature and pressure are $T = 298$ K and $P = 101325$ Pa with resulting Reynolds numbers of $Re_d = 63$, 95 and 175, respectively.

Mathematical formulation

In order to study the effects of differential diffusion in these laminar, axi-symmetric H_2/N_2 flames, the new methodology to include differential diffusion effects in CFD simulations of reactive flows, previously presented in Refs. [10,11], has been implemented in FireFOAM 1.6. (http://code.google.com/p/firefoam-dev/). The modified FireFOAM code now solves transport equations for mass, momentum, conserved scalars η_λ, and specific enthalpy, accounting for differential diffusion of species and non-unity Lewis number:

$$\frac{\partial \rho}{\partial t} + \frac{\partial (\rho u_i)}{\partial x_i} = 0 \tag{1}$$

$$\frac{\partial (\rho u_j)}{\partial t} + \frac{\partial (\rho u_i u_j)}{\partial x_i} = -\frac{\partial p}{\partial x_j} + \frac{\partial}{\partial x_i}\left(\mu\left[\frac{\partial u_i}{\partial x_j} + \frac{\partial u_j}{\partial x_i}\right]\right) + \rho g_j, \quad j = 1,2,3 \tag{2}$$

$$\frac{\partial (\rho \eta_\lambda)}{\partial t} + \frac{\partial (\rho u_i \eta_\lambda)}{\partial x_i} = \frac{\partial}{\partial x_i}\left(\rho D_{\lambda\kappa}\frac{\partial \eta_\kappa}{\partial x_i}\right), \quad \kappa, \lambda = 1, \ldots, N_e \tag{3}$$

$$\frac{\partial (\rho h)}{\partial t} + \frac{\partial (\rho u_i h)}{\partial x_i} = \frac{\partial p}{\partial t} + \frac{\partial}{\partial x_i}\left(\alpha \frac{\partial h}{\partial x_i}\right) + \sum_{k=1}^{N_s}\left(\frac{\partial}{\partial x_i}\left[h_k(\rho D_k - \alpha)\right]\frac{\partial Y_k}{\partial x_i}\right) \tag{4}$$

where ρ is the density, u is the velocity, p is the pressure, g is the gravitational acceleration, $D_{\lambda\kappa}$ are entries of the diffusion matrix and h is the specific enthalpy (sensible plus chemical).

The conserved scalars η_λ ($\lambda = 1, \ldots, N_e$) are well-chosen linear combinations of the species mass fractions Y_k ($k = 1, \ldots, N_s$). In this case N_s is the number of chemical species while N_e is the number of chemical elements considered. Linear combinations of the species mass fraction equations,

$$\frac{\partial (\rho Y_k)}{\partial t} + \frac{\partial (\rho u_i Y_k)}{\partial x_i} = \frac{\partial}{\partial x_i}\left(\rho D_k \frac{\partial Y_k}{\partial x_i}\right) + \dot{\omega}_k, \quad k = 1, \ldots, N_s \tag{5}$$

yield eq. (3), hereby canceling out the chemical source term $\dot{\omega}_k$. The species mass diffusion coefficients, D_k, are calculated as:

$$D_k = \frac{\mu}{\rho Sc_k} \tag{6}$$

where Sc_k is a constant Schmidt number of species k, assigned in this study the values $Sc_{H_2} = 0.21$, $Sc_{H_2O} = 0.63$, $Sc_{O_2} = 0.76$ and $Sc_{N_2} = 0.81$ [12]. The transformation from eq. (5) to eq. (3) gives rise to a more complex diffusion term, now featuring a complete diffusion matrix for conserved scalars $D_{\lambda\kappa}$ instead of the diagonal mass diffusion matrix for species D_k. For a more elaborate description of the transformation, we refer to [10,11].

The dynamic viscosity, μ, is a function of temperature, calculated by Sutherland's law as:

$$\mu = \frac{A_s\sqrt{T}}{1 + T_s/T} \tag{7}$$

where $A_s = 1.358519 \times 10^{-6}$ (kg/ms$\sqrt{K}$) and $T_s = 110.04$ K are the two Sutherland coefficients for the H_2/N_2 mixture [13].

The thermal diffusivity, α, is expressed as:

$$\alpha = \frac{\lambda}{c_p} \tag{8}$$

where λ is the thermal conductivity and c_p is the heat capacity at constant pressure.

The thermal conductivity is calculated by a modified Euchen formula [14]:

$$\lambda = \mu c_v[1.32 + 1.77(R/c_v)] \tag{9}$$

where c_v is the specific heat capacity at constant volume and R is the gas constant.

The specific enthalpy of species k is calculated as:

$$h_k = \underbrace{\Delta h^0_{f,k}}_{\text{chemical}} + \underbrace{\int_{T_{ref}}^{T} c_{p,k}\, dT}_{\text{sensible}} \tag{10}$$

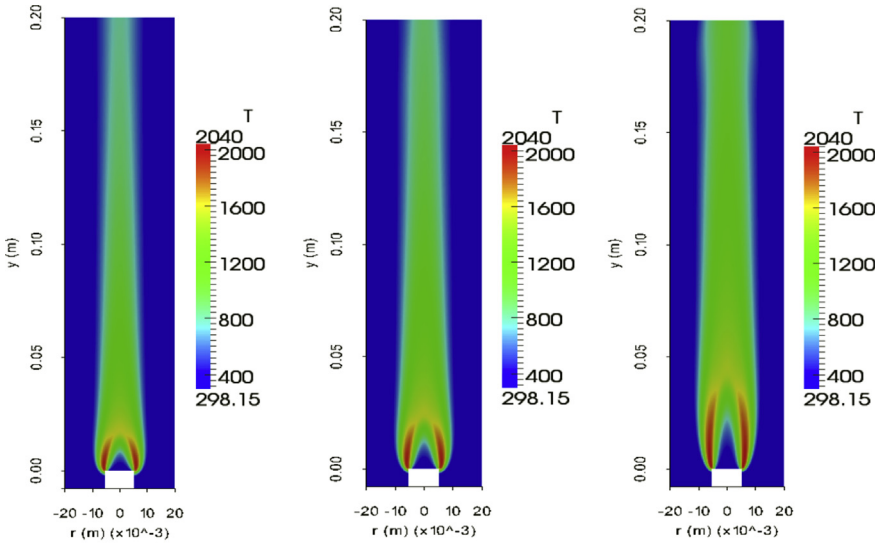

Fig. 1 – Two-dimensional snapshots of temperature distribution with differential diffusion for exit velocity of (a) 18 cm/s (T_{max} = 1984 K), (b) 27 cm/s (T_{max} = 1989 K) and (c) 50 cm/s (T_{max} = 2032 K).

where $\Delta h^0_{f,k}$ is the chemical enthalpy of formation of species k at reference temperature T_{ref} and $c_{p,k}$ is the specific heat of species k, which is temperature-dependent and calculated from the 7-coefficient NASA polynomials (Burcat database) [15]. The specific enthalpy, h, of the mixture is the sum of the specific enthalpies of all the individual species k:

$$h = \sum_{k=1}^{N_s} h_k Y_k \tag{11}$$

where Y_k is the mass fraction of species k. Temperature is then derived from specific enthalpy and species composition.

For this test case, $N_s = 4$ species k (H_2, H_2O, O_2, N_2) and $N_e = 3$ elements λ (H, O, N) are considered. The species mass fractions relate to elemental mass fractions through the Burke–Schumann solution [10,11]. In this case, differential diffusion effects are considered only in physical space (transport equations for the conserved scalars) and not in the combustion model.

Radiative heat losses were not important for these flames [7] and were therefore not included in the numerical simulations.

Numerical set-up

A cylindrical mesh is used, $11d \times 22d$, with 18 cells across the inlet. The mesh is compressed towards the centerline with a total number of 0.401 million cells, resulting in a minimum and maximum grid spacing of 0.47 mm (on the centerline) and 3.71 cm (side planes of the domain), respectively.

As mentioned, three different flames are considered in this study with exit velocities of 18, 27 and 50 cm/s. A parabolic profile is used for velocity at the inlet, similar to the one reported in the experiments, while the co-flow velocity is set to the average velocity of the fuel at the inlet. The thickness of the tube is set to 1.0 mm. At the sides of the domain, boundary conditions are of type Neumann for velocity and Dirichlet for pressure, setting the total pressure to atmospheric. At the top, a mixed boundary condition is used for velocity (Neumann if the flow is outwards, Dirichlet, imposing zero velocity, if the flow is inwards) and a Neumann condition for pressure is imposed. For the conserved scalars, all boundary conditions are of Neumann type, except for the inlet plane, where constant profiles are imposed for the fuel inlet and the co-flow.

All quantities are assigned to the cell centers (collocated grid) with velocities linearly interpolated to the cell faces. A second order central difference scheme is used for the convective and diffusive terms with a correction for the non-orthogonality of the mesh.

Results

Flame structure

The computed temperature distribution for the cases with and without differential diffusion of species and heat are presented as two-dimensional contour plots in Figs. 1 and 2. The adiabatic stoichiometric temperature of the H_2/N_2 mixture is 2040 K. As expected, substantial differences are observed. Taking into account the much higher diffusivity of H_2, the characteristic "wishbone" flame structure [16–20] is obtained. As H_2 diffuses radially outward more rapidly, the flame reaches its maximum temperature very close to the inlet, at the edges of the jet, if differential diffusion effects are taken into account. Ignoring differential diffusion effects, on the other

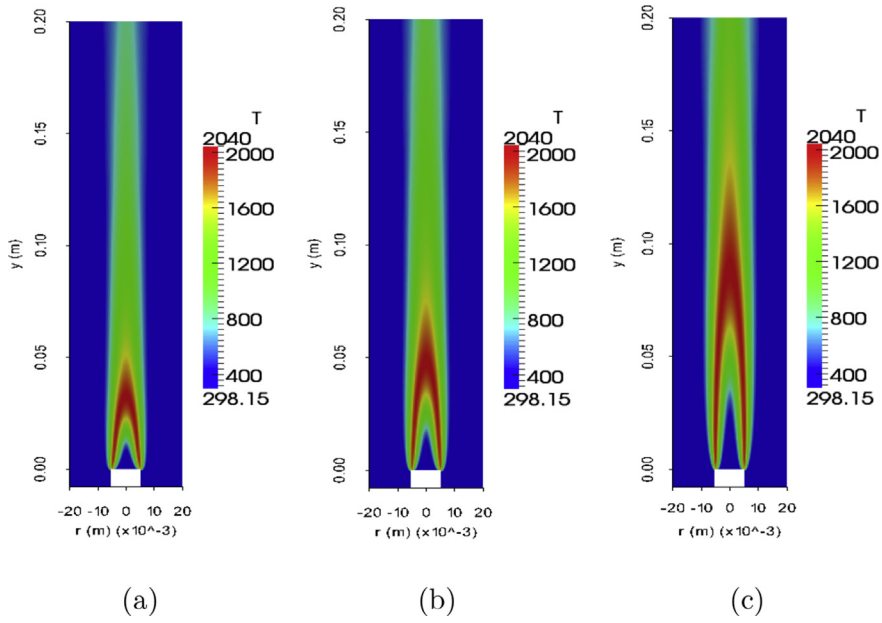

Fig. 2 – Two-dimensional snapshots of temperature distribution without differential diffusion for exit velocity of (a) 18 cm/s (T_{max} = 2035 K), (b) 27 cm/s (T_{max} = 2038 K) and (c) 50 cm/s (T_{max} = 2040 K).

hand, the rapid radially outward diffusion is not captured and the maximum flame temperature is found on the centerline. Qualitative agreement of our results (Fig. 1) and Figure 1 of Toro et al. [7] is excellent. This is quantified in the next section.

However, for completeness it is noted that the maximum flame temperatures reported in the simulations by Toro et al. [7] were 1754 K, 1817 K and 1924 K for the cases with fuel exit velocity of 18 cm/s, 27 cm/s and 50 cm/s, respectively. Our numerical results do not reveal these strong differences and the maximum temperatures are higher. This can be attributed to a number of factors. First of all, radiation is neglected in our simulations. Whereas radiation losses in hydrogen flames are known to be moderate, adiabatic calculations lead to higher temperatures. Second, we apply infinitely fast, irreversible chemical reactions in our Burke–Schumann type combustion model, while finite rate chemistry was considered in the study of Toro et al. [7], involving 9 chemical species, through the GRI 2.11 mechanism. Another possible reason for the observed differences can be attributed to reduced thermal diffusion close to the inlet in our simulations, compared to Toro's simulations. Still, this over-prediction of maximum temperature is not considered problematic. It is only a very local effect and moreover, experimental data reveal higher temperatures than the simulation results of [7] (see, e.g. Fig. 6 below). Last but not least, this issue does not interfere at all with the core story of the paper, namely the globally very good

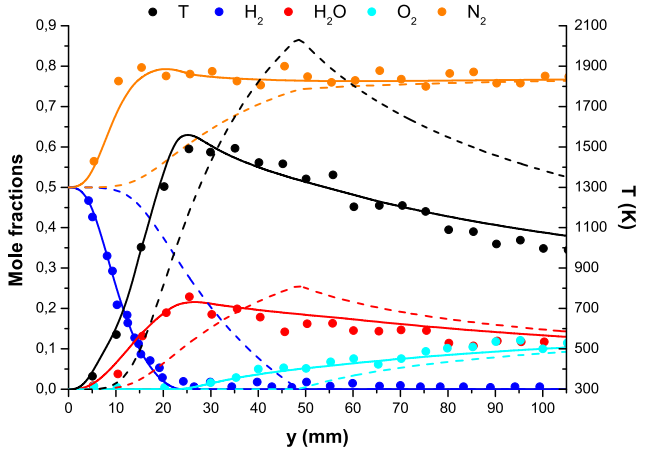

Fig. 3 – Axial temperature and species mole fractions up to y = 100 mm for 27 cm/s. Exp. data: symbols; with diff. diff.: solid lines; without diff. diff.: dashed lines.

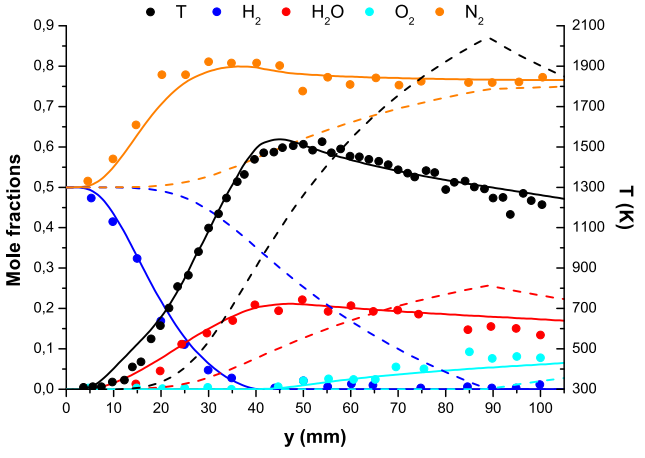

Fig. 4 – Axial temperature and species mole fractions up to y = 100 mm for 50 cm/s. Exp. data: symbols; with diff. diff.: solid lines; without diff. diff.: dashed lines.

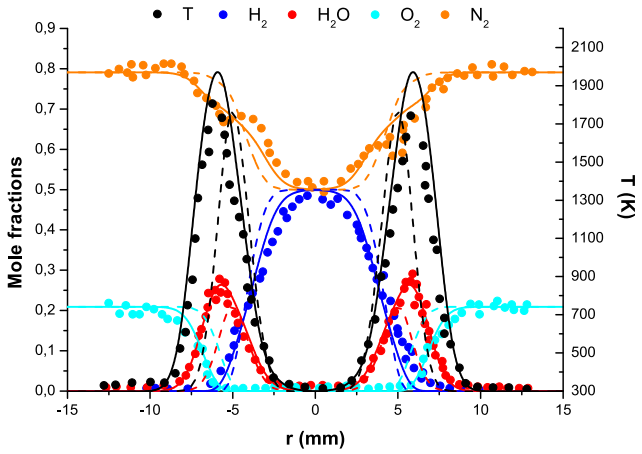

Fig. 5 – Radial temperature and species mole fractions at y = 3 mm for 50 cm/s. Exp. data: symbols; with diff. diff.: solid lines; without diff. diff.: dashed lines.

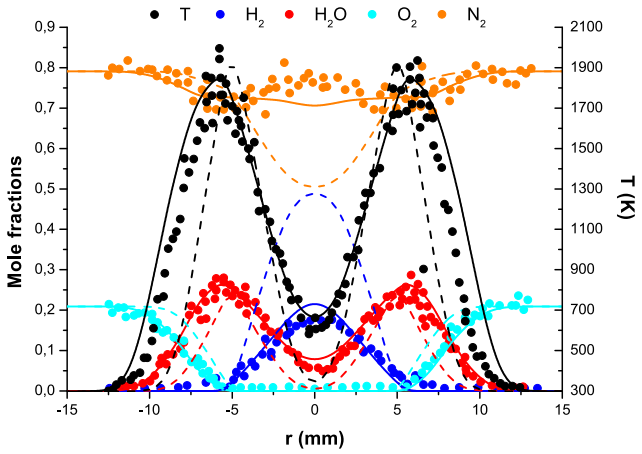

Fig. 7 – Radial temperature and species mole fractions at y = 20 mm for 50 cm/s. Exp. data: symbols; with diff. diff.: solid lines; without diff. diff.: dashed lines.

agreement of the simulation results with the present methodology to experimental data, as discussed below.

Mean results

Figs. 3–8 present results for temperature and mole fractions of species (H_2, H_2O, O_2, N_2) on the centerline up to y = 100 mm and in horizontal planes at locations y = 3, 10, 20, 30 mm. The experimental data are indicated by symbols while the results with and without differential diffusion are presented with solid and dashed lines, respectively. Black symbols correspond to temperature while blue, red, green and orange correspond to H_2, H_2O, O_2 and N_2 mole fractions, respectively.

Results for temperature and species mole fractions on the centerline at location up to y = 100 mm above the inlet for the cases with fuel exit velocities of 27 cm/s and 50 cm/s are presented in Figs. 3 and 4, respectively. It is observed that fuel is completely consumed by y = 30 mm and y = 45 mm, respectively, coinciding with the maximum values for temperature and H_2O mole fraction. The temperature profile is well captured by the simulations with differential diffusion and the same applies for the mole fractions of species mole fractions. On the other hand, if differential diffusion effects are neglected, the peak temperature on the centerline shifts much further downstream and the temperature distribution is not well captured. This leads to discrepancies in the species mole fraction results when compared with the experimental data.

Results for temperature and species mole fractions in horizontal planes at different heights y are presented below only for the case with fuel exit velocity of 50 cm/s since no experimental data are reported for the other cases in Ref. [7]. We restrict the discussion to the results with differential diffusion (although the results are presented on the figures where differential diffusion effects are ignored, for the sake of completeness).

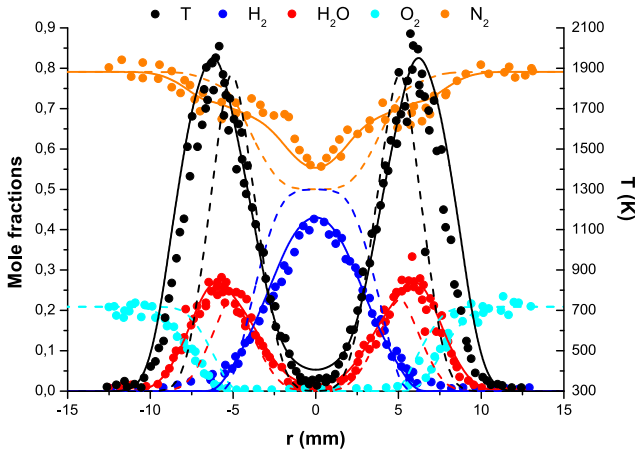

Fig. 6 – Radial temperature and species mole fractions at y = 10 mm for 50 cm/s. Exp. data: symbols; with diff. diff.: solid lines; without diff. diff.: dashed lines.

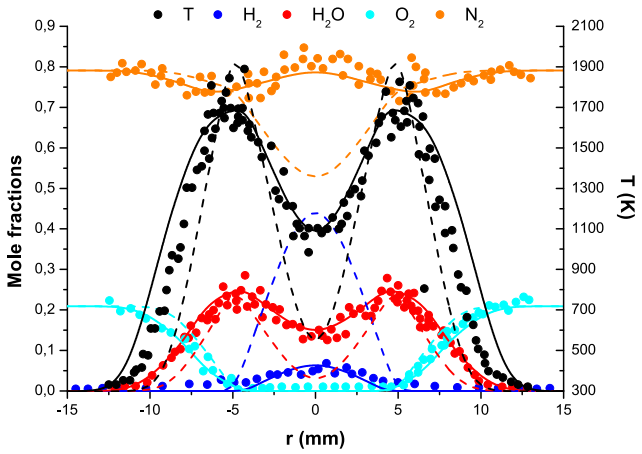

Fig. 8 – Radial temperature and species mole fractions at y = 30 mm for 50 cm/s. Exp. data: symbols; with diff. diff.: solid lines; without diff. diff.: dashed lines.

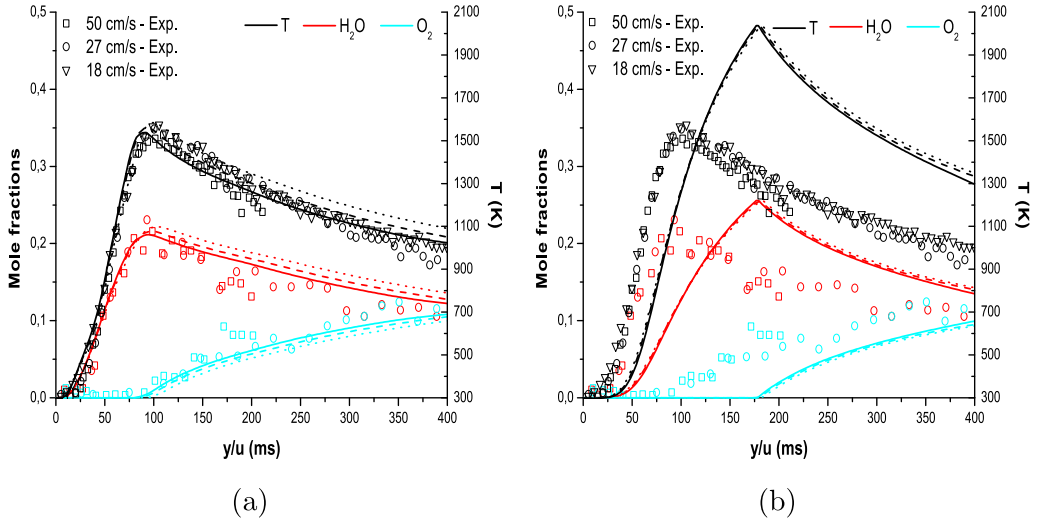

Fig. 9 – Scaled temperature and species (H_2O, O_2) profiles on the centerline (a) with and (b) without differential diffusion. Symbols: experimental data; solid lines: 50 cm/s; dashed lines: 27 cm/s; dotted lines: 18 cm/s.

At location y = 3 mm above the inlet (Fig. 5), a peak in the temperature of T = 1990 K at location x = 5.7 mm, about 1.2 mm outside the radius of the inlet is predicted. This is due to the high diffusivity of H_2 which causes the flame to stabilize at a location outside the inlet radius. A thin zone of high temperature is observed with the peaks of T and H_2O mole fraction, as expected, to coincide. The fuel rich (inner) and fuel lean (outer) sides of the jet are well predicted by the simulations and compare well with the experiments. The locally flattened profile of N_2 mole fraction, as observed in the experiments, is also reproduced to a certain extent. The peak values of H_2 and N_2 mole fractions are well predicted, although the profiles are slightly wider than the experimental ones.

At location y = 10 mm (Fig. 6), an increase in the width of the high temperature zone is observed. The peak temperature of T = 1970 K compares well with the experimental data. However, the lean side of the flame is slightly wider than the experiments. Even though the centerline temperature is still close to the ambient one, now H_2, due to its high diffusivity, has decreased, along with an increase of N_2. At this location, the locally flattened profile of N_2 mole fraction is again reproduced to a certain extent.

At location y = 20 mm (Fig. 7), an increase of the centerline temperature is observed, along with a decrease of H_2 and the diffusion of H_2O from the reaction zone to the centerline. Here, the width of the high temperature zone has increased even more when compared to y = 10 mm. The simulations with differential diffusion effects are able to predict the temperature field and the species mole fractions reasonably well, with a 22% over-prediction of H_2 on the centerline and an under-prediction of N_2. At this location, the temperature profile at the lean side of the flame is again wider when compared with the experimental data.

A further increase in the centerline temperature is observed at location y = 30 mm (Fig. 8), along with a decrease in the mole fraction of H_2. At this location, dilution with co-flow air starts to dominate the further development of the flame. Again the temperature and the species mole fractions are well captured if differential diffusion effects are taken into account.

From the previously illustrated 2D contour plots of temperature for the different flames examined (Figs. 1 and 2), it is obvious that the shape of the flame ("wishbone" flame structure) is affected by the fuel exit velocity. In Ref. [7] the temperature and species results have been normalized by the average fuel exit velocity, u, resulting in a residence time. Fig. 9 present scaled temperature and species (H_2O, O_2) results on the centerline for the cases with and without differential diffusion included. The simulated temperature and species results almost collapse. The largest differences are observed when differential diffusion is included between the case of 18 cm/s and the other two cases examined (27 cm/s and 50 cm/s), starting from the position of the maximum flame temperature and moving downstream. The experimental trends (slightly higher temperature for lower velocity) are well reproduced.

Conclusions

The novel methodology to include differential diffusion effects in CFD simulations of reactive flows, previously presented in Refs. [10,11], has been applied to a set of laminar, axi-symmetric H_2/N_2–air diffusion flames, reporting results for temperature and main species (H_2, H_2O, O_2, N_2) concentrations. Overall, very good agreement between numerical simulations and experiments has been illustrated, indicating that the proposed methodology is capable of accurately incorporating differential diffusion in numerical simulations of reactive flows when compared to other existing

methodologies (e.g. solving the species transport equations with detailed transport and chemistry [7]).

Acknowledgments

This research has been funded by Ghent University (Belgium) through BOF project 01J01909. The help of Dr. Yi Wang from FM Global concerning FireFOAM is greatly acknowledged.

REFERENCES

[1] Smith L, Dibble R, Talbot L, Barlow R, Carter C. Laser Raman scattering measurements of differential molecular diffusion in turbulent nonpremixed jet flames of H_2/CO_2 fuel. Combust Flame 1995;100:153–60.
[2] Poinsot T, Veynante D. Theoretical and numerical combustion. Philadelphia, USA: Edwards; 2005.
[3] Takagi T, Xu Z. Numerical analysis of laminar diffusion flames – effects of preferential diffusion of heat and species. Proc Combust Inst 1994;96:50–9.
[4] Takagi T, Xu Z. Preferential diffusion effects on the temperature in usual and inverse diffusion flames. Combust Flame 1996;96:252–60.
[5] Katta V, Goss L. Effects of nonunity Lewis number and finite-rate chemistry on the dynamics of a hydrogen–air jet diffusion flame. Combust Flame 1994;96:60–74.
[6] Miller J, Kee R. Chemical nonequilibrium effects in hydrogen–air laminar jet diffusion flames. J Phys Chem 1977;81:2534–42.
[7] Toro V, Mokhov A, Levinsky H, Smooke M. Combined experimental and computational study of laminar, axisymmetric hydrogen–air diffusion flames. Proc Combust Inst 2005;30:485–92.
[8] Wu C, Chen C, Li YH, Chao Y, Yuan T, Leu T. Detailed measurement and assessment of laminar hydrogen jet diffusion flames. Combust Flame 2005;146:268–82.
[9] Hancock R, Schauer F, Lucht R, Katta VR, Hsu K. Thermal diffusion effects and vortex-flame interactions in hydrogen set diffusion flames. Proc Combust Inst 1996;26:1087–93.
[10] Maragkos G, Rauwoens P, Merci B. A new methodology to incorporate differential diffusion in CFD simulations of reactive flows. Combust Flame 2013;160:1903–5.
[11] Maragkos G. A novel methodology to include differential diffusion in numerical simulations of reactive flows [Ph.D. thesis]. Ghent University; 2013.
[12] Giacomazzi E, Picchia F, Arcidiacono N. A review of chemical diffusion: criticism and limits of simplified methods for diffusion coefficient calculation. Comb Theory Model 2008;12:135–58.
[13] Saxena S. Viscosity of multicomponent mixtures of gases. In: Proceedings of the 6th symposium on thermophysical properties; 1973. pp. 100–10.
[14] Bird R, Stewart W, Lightfoot E. Transport phenomena. New York, USA: John Wiley and Sons, Inc.; 1960.
[15] Burcat A. Thermochemical data for combustion calculations. John Wiley & Sons; 1984 [Ch. 8 in Combustion chemistry].
[16] Northrup S, Groth C. Solution of laminar combusting flows using a parallel implicit adaptive mesh refinement algorithm. Comp Fluid Dyn 2009;4:341–6.
[17] Mohammed R, Tanoff M, Smooke M. Computational and experimental study of a forced, timevarying, axisymmetric, laminar diffusion flame. Proc Combust Inst 1998;27:693–702.
[18] Mokhov A, Bennett B, Levinsky H, Smooke M. Experimental and computational study of C_2H_2 and CO in a laminar axisymmetric methane–air diffusion flame. Proc Combust Inst 2007;31:997–1004.
[19] Bennett B, McEnally C, Pfefferle L, Smooke M. Computational and experimental study of axisymmetric coflow partially premixed methane–air flames. Combust Flame 2000;23:522–46.
[20] Smooke M, Xu Y, Zurn R, Lin P, Frank J, Long M. Computational and experimental study of OH and CH radicals in axisymmetric laminar diffusion flames. Proc Combust Inst 1992;24:813–21.